Attractive interatomic force as a tunnelling phenomenon

1991 J. Phys.: Condens. Matter 3 1227

(http://iopscience.iop.org/0953-8984/3/10/002)

J. Phys.: Condens. Matter 3 (1991) 1227–1245. Printed in the UK

Attractive interatomic force as a tunnelling phenomenon

C Julian Chen
IBM Thomas J Watson Research Center, PO Box 218, Yorktown Heights, NY 10598, USA

Received 3 August 1990

Abstract. Based on time-dependent perturbation theory, we established a fundamental equality between Bardeen's tunnelling matrix element and Heisenberg's resonance energy. Applying this equality to the hydrogen molecular ion, we derived a simple analytic expression for the potential curves in the attractive-force regime, which is found to be accurate to better than 1×10^{-4} au throughout the entire regime. By extending it to the many-body case, we present a unified view of scanning tunnelling microscopy (STM) and atomic force microscopy (AFM). The fundamental equality then has a measurable consequence: for metals, the observed attractive atomic force F and the observed tunnelling conductance G should conform to the general equation $F = -f\kappa\varepsilon(GR_K)^{1/2}$, where κ is the inverse decay length of the surface wavefunction near the Fermi level, ε is the width of the conduction band of the metal, R_K is von Klitzing's constant and f is a dimensionless factor of the order of unity, which depends on tip geometry. The equation is found to be in quantitative agreement with recent results of combined experiments of AFM and STM. Conceptually, it means that the imaging process in STM is a sequence of bond forming and bond rupturing. From the computational point of view, the equality between Bardeen's tunnelling matrix element and Heisenberg's resonance energy may open a new first-principles method for calculating potential curves of molecules and the exchange coupling responsible for magnetism.

1. Introduction

Since the invention of scanning tunnelling microscopy [1] (STM) and atomic force microscopy [2] (AFM), for the first time in history, individual atoms on surfaces, individual electronic states of atomic dimensions as well as forces with atomic-scale resolution become directly perceptible. From the instrumentation point of view, STM and AFM are based on very similar concepts. The underlying processes, i.e. the tunnelling conductance and the interatomic force, have been considered as fundamentally unrelated. Nevertheless, recently, a series of interesting experimental and theoretical results [3–6] showed that the interatomic force and tunnelling conductance are closely related. These are now briefly outlined.

1.1. Measured tip–sample distance

Because of the observed exponential dependence of tunnelling conductance with distance, in the early years of STM experiments, only the *relative* tip–sample distances were measured. The absolute distance was estimated [7] to be about 10 Å. The argument

0953-8984/91/101227 + 19 $03.50

was based on the observed exponential dependence of tunnelling conductance on distance, which seems to imply a WKB behaviour, with a tunnelling barrier roughly equal to the vacuum level. This could happen only when the barrier lowering due to image force is small, which implies a distance at least as large as 6 Å. However, recent direct measurements of the tip–sample distance have revealed a dramatic deviation from this early concept. With a combined AFM-STM experiment on metals, Dürig *et al* have shown [3] that, under normal experimental conditions in STM, the tip–sample distances are 1–4 Å before mechanical contact. With a tungsten tip, on a silicon surface, the normal tip–sample separation is measured to be about 3 Å before mechanical contact [5]. The distance of mechanical contact is defined as the distance where the net force between the tip and the sample is zero, that is, where the attractive force equals the repulsive force. Finally, in order to understand the very basic experimental fact of STM, the atomic resolution, such a short tip–sample distance is a necessary condition [6]. Hence, the range of tip–sample distances under normal STM operation coincides with the range of strong attractive force between tip and sample [4, 5].

1.2. Exponential dependence of attractive force with distance

The same experiments of Dürig *et al* revealed that, in the attractive-force regime, the observed atomic force obeys an exponential law with respect to tip–sample separation [3] over a range of 3 Å. The range of the exponential attractive force overlaps with that of normal STM operation [3]. The exponential dependence indicates that the nature of the force cannot be van der Waals. Furthermore, the magnitude of the force is much larger than the theoretical value of the van der Waals force [8, 9]. Dürig *et al* attribute the observed attractive force to *metal adhesion*, a macroscopic phenomenon based on the overlap of electron wavefunctions of the same and the tip, which has the right magnitude and the right exponential dependence [10].

1.3. Effect of force in STM experiments

The force occurring during STM experiments may deform the tip as well as the sample, and thus affect the observed images. This was first proposed by Soler *et al* then verified and extended by many other authors [4]. Attractive force also plays a vital role in STM experiments, especially in the measurement of apparent barrier heights. The force may result in deformation of the sample as well as the tip [4]. The actual displacement of the tip–sample separation may differ from the measured z-piezo displacement. The apparent barrier height as measured through the z-piezo displacement can differ from the apparent barrier height by definition [5].

1.4. Outline of this paper

To summarize, experimental evidence shows that, in the range of normal operation of STM, attractive force always accompanies tunnelling [3–6]. Therefore, an understanding of the relation between atomic force and tunnelling conductance is important for the understanding of both STM and AFM.

To date, most of the theoretical work on AFM attributed the force to van der Waals interactions [9]. This is in accordance with the earlier estimation of the tip–sample separation [7], i.e. greater than 6 Å. This distance, however, excludes the possibility of achieving atomic resolution [7], and contradicts the recent direct measurement of the

normal tip–sample separation [3, 5], 1–4 Å before mechanical contact. We will show that, at normal tip–sample distances, the wavefunctions of the tip and the sample exhibit substantial overlap, and the resonance energy [11] becomes much greater than the van der Waals energy, which means that the attractive force occurring in normal STM operation is predominantly due to resonance energy.

The problem here is of a very fundamental nature. To elucidate it, using the time-dependent Schrödinger equation, we show that for two atomic systems weakly coupled, Bardeen's tunnelling matrix element [12] and Heisenberg's resonance energy [13] are equal. By applying this fundamental equality to the problem of the hydrogen molecular ion [11], we show that in the entire range of attractive force the coupling energy can be accurately represented as a sum of the van der Waals energy [8] and the resonance energy [13, 14]. By evaluating the resonance energy using Bardeen's expression for the tunnelling matrix element [12], an exceedingly accurate analytic expression for the potential curve of the hydrogen molecular ion is derived.

By extending this fundamental relation to the many-body case, we show that the interatomic force in the attractive-force regime and the tunnelling conductance are intrinsically related. For metals, an explicit equation between two sets of *measurable quantities* is derived. These quantities can be directly and independently determined using STM and AFM. A comparison with recent experiments [3] shows good agreement. Conceptually, the new theory implies that in the distance range of normal STM operations, the atom-resolved STM imaging process can be considered as a sequence or bond forming and bond rupturing.

From the point of view of computational physics, the equality between Bardeen's tunnelling matrix element and Heisenberg's resonance energy may open a new first-principles method for calculating potential curves in molecules and exchange energies responsible for magnetism using perturbation method. The concept of resonance is the foundation of Pauling's theory of chemical bonds [14]. Actually, by expanding the wavefunction in terms of spherical harmonics, Bardeen's tunnelling matrix elements follow an extremely simple *derivative rule* [6]. Because the resonance energy exactly equals Bardeen's integral, analytical expressions for the potential curves at larger distances can be obtained. In many cases, the exchange constants occurring in magnetism are within the range of pure attractice interatomic force. Therefore, the analytic method of evaluating Bardeen's tunnelling matrix elements may open a new way of calculating or estimating these coupling constants.

Because this paper is written for experimentalists as well as theorists, two unit systems are used in parallel. In discussing theoretical issues, atomic units (au) are used: energy in hartrees (≈27.21 eV), length in bohrs (≈0.529 Å). In discussing experimental issues, electron volts and ångströms are used. The unit of force, nN, is related to these units through the following relations:

$$1\ \text{eV}/1\ \text{Å} \simeq 1.60\ \text{nN}$$

$$1\ \text{Hartree}/1\ \text{Bohr} \simeq 82.3\ \text{nN}.$$

2. Hydrogen molecular ion revisited

In quantum mechanics as well as in field theory, solvable models are always precious. For example, the hydrogen molecular ion is one of the most important solvable problems

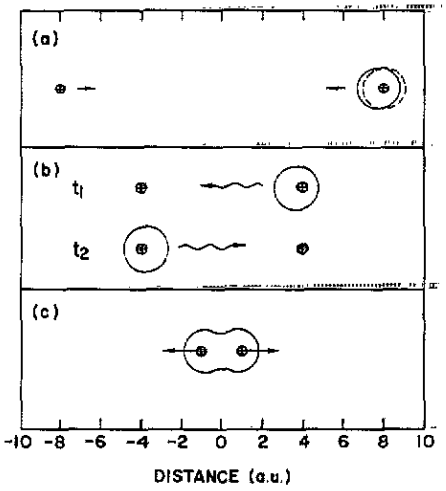

Figure 1. Three regimes of interaction of a hydrogen atom with a proton. (*a*) At large distances, $R > 16$ au, the system can be considered as a neutral hydrogen atom plus a proton. The polarization of the hydrogen atom due to the field of the proton generates a van der Waals force. (*b*) At intermediate distances, 16 au $> R > 4$ au, the electron can tunnel to the vicinity of another proton, and vice versa. A resonance force is generated, which is either attractive or repulsive. (*c*) At short distances, $R < 4$ au, proton–proton repulsion becomes important.

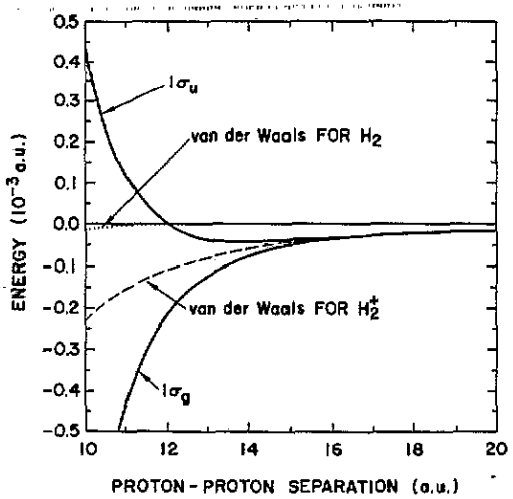

Figure 2. A comparison of the van der Waals energy and the resonance energy for the hydrogen molecular ion at relatively large distances. The van der Waals energy for a pair of neutral hydrogen atoms is also shown.

in quantum mechanics because 'a great many of the properties of molecules are illustrated in this simple case', as Slater opens his four-volume *Quantum Theory of Molecules and Solids* with a details treatment of it [11].

In this section, we present a new interpretation of the exact solution of the H_2^+ problem in terms of tunnelling [12]. We will show that a great many of the properties of STM and AFM can be illustrated in this simple case.

2.1. Three regimes of interaction

Figure 1 shows three regimes of interaction in a hydrogen molcular ion. At large distances, the system can be considered as a neutral hydrogen atom plus a proton. The electrical field of the proton polarizes the hydrogen atom. As a result, a van der Waals force is induced [8]. The van der Waals force dominates as the proton–proton distance $R > 8$ Å. At a distance $R < 8$ Å, the 1s electron at the vicinity of the right proton has an appreciable probability to tunnel into the 1s state of the left proton, and vice versa. The tunnelling phenomenon gives rise to a *resonance* and results in a lowering of the total energy [13]. The concept of such resonance was suggested by Heisenberg [13] in 1926 for treating many-body problems. It is also the foundation of Pauling's theory of the chemical bond [14]. The resonance gives rise to a bonding state with a lower total energy (attractive force) and an antibonding state with a higher total energy (repulsive force).

At even shorter distances, e.g. $R < 2.5$ Å, the repulsive force between the protons becomes important, and the net force becomes repulsive regardless of the type of state.

In the following, we discuss the three regimes individually.

2.2. *Van der Waals force*

As shown in figure 1(*a*), at large distances, the system can be considered as a neutral hydrogen atom plus an isolated proton. The field of the proton polarizes the hydrogen atom to induce a dipole. The interaction between the proton and the induced dipole generates a van der Waals force. The van der Waals force can be treated as a classical phenomenon [8] by introducing a pheonomenological polarizability α:

$$p = \alpha E \tag{2.1}$$

where p is the induced dipole of the neutral hydrogen atom, and E is the electrical field of another proton. The coupling energy E between the proton and the neutral hydrogen atom is [8]

$$E = -(\alpha/2)R^{-4}. \tag{2.2}$$

The polarizability of the hydrogen atom can be calculated accurately using quantum mechanics. To a high degree of accuracy, the effect can be described as follows. A p_z component is induced by the external electric field, which in turn generates a shift of the centre of negative charge from the position of the proton [15]. This p_z component is of the same nature as the tip-induced local states (TILS) in the theory of STM introduced by Ciraci *et al* [16]. The accurate evaluation of the polarizability is one of the earliest applications of quantum mechanics. Using parabolic coordinates [17], it was shown that $\alpha = 9/2$. Therefore,

$$E = -\tfrac{9}{4}R^{-4}. \tag{2.3}$$

For the situation in STM and AFM, the above treatment, i.e. the van der Waals force between a neutral hydrogen atom and a proton, represents a gross overestimation. Actually, in STM and AFM experiments of conducting materials, the features near the gap are nearly neutral, which is similar to the situation of a pair of neutral hydrogen atoms rather than a proton with a neutral hydrogen atom. The van der Waals force between a pair of neutral hydrogen atoms is also a well studied problem. The accurate result is [8]

$$E = -6.50R^{-6}. \tag{2.4}$$

For values of R of interest, the van der Waals force between neutral atoms is about one order of magnitude smaller than the case of a neutral atom and an ion. A comparison of these two cases is shown in figure 2. As shown, in the range of interest, both are much smaller than the typical bonding energy of diatomic molecules—a few electron volts.

2.3. *Resonance energy due to tunnelling*

As shown in figure 1(*b*), at a shorter proton–proton separation ($R < 16$ au or $R < 8$ Å), the electron in the 1s state in the vicinity of one proton has an appreciable probability to tunnel to the 1s state in the vicinity of another proton. The tunnelling matrix element can be evaluated using perturbation theory similar to those of Oppenheimer [18] and Bardeen [12]. A schematic is shown in figure 3. By defining a pair of one-centre potentials, U_L and U_R, we define the right-hand-side states and the left-hand-side states.

Because the potential U_L is different from the potential of a free proton, U_{L0}, the wavefunction ψ_L and the energy level E_0 different from the 1s state of a free hydrogen atom. (The same is true for U_R and ψ_R.) We will come back to the effect of such a distortion later in this section.

In the following, we present a treatment of the hydrogen molecular ion problem using the time-dependent Schrödinger equation:

$$i\partial\Psi(r,t)/\partial t = (-\tfrac{1}{2}\nabla^2 + U)\Psi(r,t) \tag{2.5}$$

where U is the potential curve for the hydrogen molecular ion, as shown in figure 3(a). Similarly, for the left-hand-side and right-hand-side problems, we also look for solutions of corresponding time-dependent Schrödinger equations:

$$i\partial\Psi_L(r,t)/\partial t = (-\tfrac{1}{2}\nabla^2 + U_L)\Psi_L(r,t) \tag{2.6}$$

$$i\partial\Psi_R(r,t)/\partial t = (-\tfrac{1}{2}\nabla^2 + U_R)\Psi_R(r,t). \tag{2.7}$$

We denote the ground-state solutions of equations (2.6) and (2.7) as

$$\Psi_L(r,t) = \psi_L(r)\exp(-iE_0t) \tag{2.8}$$

$$\Psi_R(r,t) = \psi_R(r)\exp(-iE_0t). \tag{2.9}$$

Because of time-reversal symmetry, the functions $\psi_L(r)$ and $\psi_R(r)$ can always be made real. Also, since the ground-state wavefunction does not have a node, we can always make the values of wavefunctions everywhere positive. Now, we look for solutions of equation (2.5) that are linear combinations of the solutions of equations (2.6) and (2.7). In other words, we make the following *ansatz*:

$$\Psi(r,t) = a_L(t)\psi_L(r)\exp(-iE_0t) + a_R(t)\psi_R(r)\exp(-iE_0t). \tag{2.10}$$

Substitute equation (2.10) into equation (2.5), using the relations

$$U = U_L + U_R \tag{2.11}$$

$$U_LU_R = 0 \tag{2.12}$$

time-dependent perturbation theory gives the following equations:

$$\dot{a}_L(t) = iMa_R(t) \tag{2.13}$$

$$\dot{a}_R(t) = iMa_L(t). \tag{2.14}$$

The transmission matrix element M can be expressed as the Bardeen integral

$$M = \frac{1}{2}\int(\psi_R\nabla\psi_L - \psi_L\nabla\psi_R)\cdot dS \tag{2.15}$$

which is evaluated on the separation surface, i.e. the median plane (see figure 3). The details of the derivation are shown in the appendix. We use the convention that the gradient ∇ along the z direction means $+\partial/\partial z$. The behaviour of the wavefunctions reveals immediately that the matrix element is real and *negative*.

A specific solution of equation (2.5) now depends on the initial condition. If at $t = 0$ the electron is in the left-hand-side state, the solution is

$$\Psi_1(r,t) = [\cos(Mt)\psi_L(r) + i\sin(Mt)\psi_R(r)]\exp(-iE_0t). \tag{2.16}$$

This solution describes a back-and-forth migration of the electron between the two

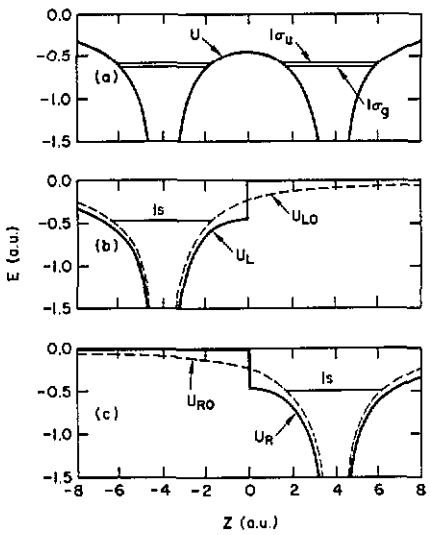

Figure 3. Perturbation treatment of the hydrogen molecular ion. (*a*) The exact potential curve and the exact energy levels of the problem. (*b*) Full curve, the left-hand-side potential for a perturbation treatment; broken curve, the potential for a free hydrogen atom. (*c*) Full curve, the right-hand-side potential for a perturbation treatment; broken curve, the potential for a free hydrogen atom. Distance is in atomic units (1 au = 0.539 Å) and energy is also in atomic units or hartrees (1 au = 27.21 eV).

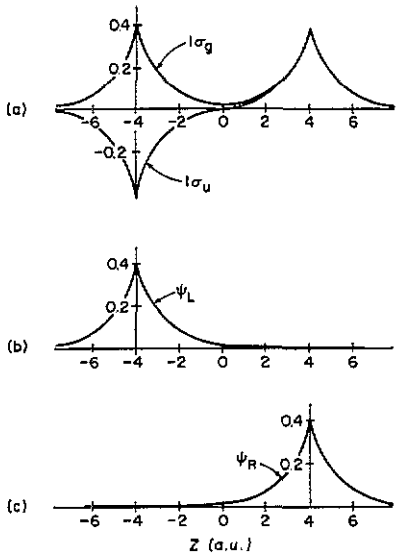

Figure 4. (*a*) The exact wavefunctions of the hydrogen molecular ion. Two lowest states are shown. The two exact solutions can be considered as symmetric and antisymmetric linear combinations of the solutions of the left-hand-side and right-hand-side problems, (*b*) and (*c*), defined by potential curves in (*b*) and (*c*).

protons. At $t = 0$, the electron is revolving about the left-hand-side proton with a frequency $f = |E_0|/h$. Then, the electron starts migrating to the right-hand side. At $t = \pi/|M|$, the electron has migrated entirely to the right-hand side; and at $t = 2\pi/|M|$, the electron comes back to the left-hand side, etc. In other words, the electron migrates back and forth between the two protons with a frequency $\nu = |M|/h$. Similarly, we have another solution:

$$\Psi_2(r, t) = [\cos(Mt)\psi_R(r) + \mathrm{i}\sin(Mt)\psi_L(r)]\exp(-\mathrm{i}E_0 t) \tag{2.17}$$

which starts with a right-hand side state at $t = 0$.

The linear combinations of the solutions, equations (2.16) and (2.17), are also good solutions of the time-dependent Schrödinger equation, equation (2.5). For example, there is a state symmetric with respect to space:

$$\Psi_g(r, t) = \Psi_1 + \Psi_2 = [\psi_L(r) + \psi_R(r)]\exp[-\mathrm{i}(E_0 + M)t] \tag{2.18}$$

as well as an antisymmetric state:

$$\Psi_u(r, t) = \Psi_1 - \Psi_2 = [\psi_L(r) - \psi_R(r)]\exp[-\mathrm{i}(E_0 - M)t]. \tag{2.19}$$

For brevity, the normalization constant is omitted. Obviously, these solutions are

stationary states of equation (2.5) with energy eigenvalues $E_0 + M$ and $E_0 - M$, respectively. Because both E_0 and M are negative, the symmetric state has a lower energy, which means an attractive force.

The above discussion is but another formulation of the concept of *resonance* introduced by Heisenberg [13] for treating many-body problems in quantum mechanics. Heisenberg illustrated this concept with a classical mechanical model [13]: two similar pendulums connected by a weak spring. Accordingly, the meaning of equation (2.16) is as follows. At $t < 0$, the right-hand-side pendulum is held still, and the left-hand-side pendulum is set to oscillate with a frequency $|E_0|/h$. At $t = 0$, the right-hand-side pendulum is released. Because of the coupling through the weak spring, the left-hand-side pendulum gradually ceases to oscillate, transferring its momentum to the right-hand-side pendulum, which now begins its oscillation. At $t = \pi/|M|$, the right-hand-side pendulum reaches the maximum amplitude, and the left-hand-side pendulum stops. Then, the process reverses. This mechanical system has two normal modes, with the two pendulums oscillating in the opposite directions or in the same direction, with frequencies $|E_0 + M|/h$ and $|E_0 - M|/h$, respectively. These two normal modes correspond to the symmetric and antisymmetric states of the hydrogen molecular ion, respectively, as shown in figure 4. The two curves in figure 4(a) are the exact solutions of the two low-energy solutions of the H_2^+ problem [11]. To a good approximation, these solutions can be represented by the symmetric and antisymmetric superpositions of the distorted hydrogen wavefunctions, as shown in figures 4(b) and (c). These wavefunctions are defined by the left-hand-side and right-hand-side potentials (figures 3(b) and (c)).

In the following, we show that by expressing the tunnelling matrix element, and consequently Heisenberg's resonance energy, as a Bardeen integral [12], with the distortion of the hydrogen wavefunction considered [19], an exceedingly accurate analytic expression for the exact potential of the hydrogen molecular ion is obtained.

Before we proceed to make an explicit evaluation of the Bardeen integral, we make a brief discussion about the effect of the distortion potentials, e.g. $\Delta U = U_L - U_{L0}$. The value of ΔU at the centre of the left-hand-side proton results in an increase of total energy due to the repulsive force between the protons, which is exactly cancelled by the attractive force between the right-hand-side proton and the electron in its undistorted state. The gradient of ΔU in the z direction induces a shift of the centre of the electron wavefunction, which is the origin of the van der Waals force, as we have discussed above [8]. For relatively large distances, to a good approximation, equation (2.3) should still be accurate. The distortion potential also increases the absolute value of wavefunction on the median plane, with respect to the wavefunctions of the free hydrogen atoms which makes the tunnelling matrix element, equation (2.16), larger than what would be expected from the wavefunction of a free hydrogen atom [19].

The effect of distortion as well as the evaluation of the integral (2.16) has been discussed by Holstein regarding the charge-exchange interaction between ions and parent atoms [19]. Holstein [19] showed that the net effect of the distortion on the wavefunction at the separation surface is a constant multiplier, $g = 2\exp(-1/2) \approx 1.213$. Holstein's integral, which represents the *energy splitting* between the symmetric state and the antisymmetric state, has the value [19]

$$E(1\sigma_u) - E(1\sigma_g) = -\int (\psi_R \nabla\psi_L - \psi_L \nabla\psi_R) \cdot dS = (4/e)R\exp(-R). \tag{2.20}$$

Holstein's integral is exactly twice the minus value of Bardeen's tunnelling matrix

Table 1. Energy eigenvalues of the hydrogen molecular ion: a comparison between the accurate values tabulated in [20] and the analytic expression (2.24). Energy in rydbergs (1 Ryd = 0.5 Hartree ≃ 13.6 eV).

R	$-E(1\sigma_g)$ (Ryd)			$-E(1\sigma_u)$ (Ryd)		
(au)	[20]	(2.24)	Difference	[20]	(2.24)	Difference
6.0	1.35726	1.35869	0.00143	1.31462	1.31492	0.00030
6.5	1.32412	1.32459	0.00047	1.29581	1.29583	0.00002
7.0	1.29690	1.29698	0.00008	1.27826	1.27820	−0.00006
7.5	1.27426	1.27419	−0.00007	1.26206	1.26198	−0.00008
8.0	1.25514	1.25505	−0.00009	1.24721	1.24715	−0.00006
8.5	1.23878	1.23870	−0.00008	1.23365	1.23361	−0.00004
9.0	1.22461	1.22454	−0.00007	1.22131	1.22127	−0.00004

element [12] with the distortion included, i.e. equation (2.15). Therefore, we obtain the value of the integral in equation (2.15):

$$M = -(2/e)R\exp(-R). \tag{2.21}$$

As we have shown, the resonance energy of Heisenberg [13] and Pauling [14] is exactly equal to this tunnelling matrix element [12]. The total coupling energy is the sum of the van der Waals energy [8] and the resonance energy [13]. For the $1\sigma_g$ state, it is

$$\Delta E(1\sigma_g) = -\tfrac{9}{4}R^{-4} - (2/e)R\exp(-R) \tag{2.22}$$

and for the $1\sigma_u$ state

$$\Delta E(1\sigma_u) = -\tfrac{9}{4}R^{-4} + (2/e)R\exp(-R). \tag{2.23}$$

Table 1 shows a comparison between equations (2.22)–(2.23) and the exact solution of the H_2^+ problem. To make a direct comparison to the tabulated results of the exact solution [20] published by Bates *et al*, we noticed that in the numbers of their tables, the energy reference is the vacuum, the Coulomb repulsion energy of the two protons is not included, and rydbergs (1 Ryd ≡ 0.5 Hartree ≃ 13.6 eV) is used as energy unit [20]. In this form, equations (2.22)–(2.23) becomes†

$$E_\pm = -1 - 2/R - \tfrac{9}{2}R^{-4} \pm (4/e)R\exp(-R) \qquad \text{(Ryd)}. \tag{2.24}$$

As shown in table 1, in the range $R > 6$ au, or $R > 3$ Å, the agreement is exceedingly good. It should be emphasized that equation (2.24) is based on pure theoretical reasoning with no adjustable parameters. Therefore, the interpretation of the resonance energy in terms of tunnelling is illustrated quantitatively in the case of the hydrogen molecular ion.

In the paper of Bates *et al* [20], the exact numerical results are listed up to $R = 9$ au. Because the approximate solution (2.24) is exceedingly accurate in the entire range of $R \simeq 6$–9 Å, it is expected to be equally accurate for $R > 9$ au. In figure 2, a comparison of the van der Waals energy and the resonance energy in the large-distance ($R > 10$ au) regime is shown. At $R > 16$ au, the van der Waals force dominates. As $R < 16$ au, the

† Equations (2.22) through to (2.24) might have been discovered many years ago. Being unsuccessful in finding them in any literature, the author would appreciate any information about a proper reference.

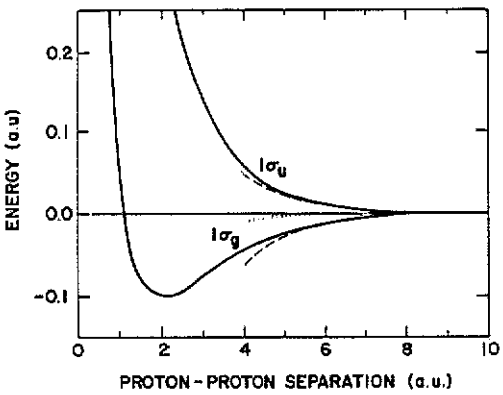

Figure 5. Comparison of the exact solution of the hydrogen molecular ion problem (full curves) with the approximate equations in the attractive-force regime (broken curves) after equation (2.24). At short distances, the proton–proton repulsion becomes important, which results in the discrepancy between the exact solution and the asymptotic expression, equation (2.24). The van der Waals component, equation (2.3), is also shown as a dotted curve.

resonance energy becomes important. It is interesting to note that even for the $1\sigma_u$ state, there is a shallow minimum at about $R = 14$ au, or 7 Å. The absolute value, 4.1×10^{-5} au, or 1.1 meV, is much smaller than the typical values of resonance energy, a few eV. At $R = 10$ au, the resonance energy is already much larger than the van der Waals energy.

A comparison of the approximate equation (2.24) with the exact potential curves of H_2^+ in the short-distance regime is shown in figure 5. Notice that the vertical scale in figure 5 is about 1000 times larger than that in figure 2. The van der Waals energy is almost imperceptible on this scale. The resonance energy, equation (2.21), describes the asymptotic behaviour of the exact potential well down to about 4 au. At even shorter distances, e.g. $R < 4$ au, core–core repulsion becomes important.

2.4. Core–core repulsion

As shown in figure 1, as the proton–proton separation becomes even smaller, the picture of resonance becomes obscured, and the proton–proton repulsion is no longer screened by the electron. Slater [11] has shown that the Morse curve can fit very well to the exact potential curve. The Morse curve can be considered as a sum of an exponential attactive force and an exponential repulsive force, which is intuitively understandable and analytically simple.

2.5. An order-of-magnitude comparison

To assess the relative importance of the van der Waals and the resonance components occurring in STM and AFM, it is instructive to compare the quantities occurring in real experiments versus those quantities in the exactly solvable H_2^+ problem.

2.5.1. The range of separation. The experimentally determined tip–sample separation is 1–4 Å before mechanical contact [3, 5]. In the case of H_2^+, the proton–proton separation at mechanical contact, i.e. the point with zero net force [11], is 2 au or 1.06 Å. Therefore, the range of normal STM operation corresponds to a nucleus–nucleus separation of 2–5 Å, or 4–10 au in the case of the hydrogen molecular ion. This is exactly the range within which the resonance interaction [13] dominates, and the approximate expression (2.24) provides an accurate description of the total atomic force. In this

Table 2. A comparison of the resonance energy with the van der Waals energies for the hydrogen molecular ion ($H + H^+$) and neutral hydrogen molecule ($H + H$). The actual situation in STM and AFM, in terms of van der Waals force, is similar to that of two neutral atoms. The ratio of the van der Waals energy with respect to the resonance energy is also shown. For the case of practical interest, i.e. the neutral atoms, the van der Waals energy is less than 2% of the total bonding energy.

R (au)	Resonance (au)	van der Waals (H_2^+) (au)	Ratio (%)	van der Waals (H_2) (au)	Ratio (%)
5.0	0.024788	0.003600	14.5	0.000416	1.7
6.0	*0.010943*	*0.001736*	*15.9*	*0.000139*	1.3
7.0	0.004696	0.000937	20.0	0.000055	1.2
8.0	0.001975	0.000549	27.8	0.000025	1.3
9.0	0.000817	0.000343	42.0	0.000012	1.5

range, both van der Waals force and the repulsive force are much smaller than the resonance force, as shown in table 2. In other words, under normal STM operation conditions, over a distance range of about 3 Å, *resonance energy is almost solely responsible for the atomic force*, and the distance dependence of the force should be approximately exponential.

2.5.2. The sensitivity of AFM. In the best AFM experiments [2], the force sensitivity is about 0.01 nN. In the range of 4–10 au, the resonance force in the hydrogen molecule ion is 4 to 0.01 nN. Therefore, the resonance force (attractive atomic force) of a single chemical bond, extended over a distance of 3 Å, can be detected. On the other hand, the van der Waals force of a pair of neutral atoms, when it is distinguishable from the total force, is always smaller than 0.01 nN, which is beyond the detection limit of the existing AFM. On the other hand, the *repulsive force*, when it is separable from the resonance force, can be as large as some tens of nanonewtons, which is always within the detection limit of AFM.

2.6. Comparison with previous work

Perturbation treatments for the atomic force have been discussed by Holstein [19] in conjunction with charge-exchange interactions as well as Flores *et al* [21] in conjunction with STM. Holstein's theory [19] deals with the *energy splitting* between the bonding and antibonding state, not the actual bonding energy, i.e. the lowering of the ground-state energy of two systems relative to its energy at infinite separation [19]. Holstein derived an accurate asymptotic equation for the value of energy splitting between the lowest bonding state ($1\sigma_g$) and the lowest antibonding state ($1\sigma_u$) of the hydrogen molecular ion, with the effect of distortion included [19]. Here, we show that the total binding energy can be accurately represented as a sum of the van del Waals energy and the resonance energy, and the latter exactly equals one-half of Holstein's value of energy splitting. Flores *et al* considered the problem of STM using a muffin-tin model and reached a similar equation [21] for the interaction, without considering the distortion due to another party. They interpret their result as a relation between the tunnelling *current* and the *repulsive* atomic force. In the following section, we show that the equality

between Bardeen's tunnelling matrix element and Heisenberg's resonance energy leads to an explicit equation between the tunnelling *conductance* and the *attractive* atomic force, which can be verified by direct and independent measurements.

3. Attractive atomic force on metal surfaces

The goal of this section is to establish a general equation between the attractive atomic force and the tunnelling conductance on metal surfaces, as a result of the equality between Bardeen's tunnelling matrix element and Heisenberg's resonance energy. This equation is valid only in the range of tip–sample distances where the exchange force dominates. Such a range of tip-sample distances coincides with the normal operating conditions of STM.

3.1. Van der Waals force

The van der Waals force between two solid bodies is a well studied problem [8]. Because the van der Waals force is a valid description of the interatomic forces between two pieces of solid with a distance much larger than the diameter of a typical atom, a macroscopic approach is often used [8]. The results show that the force between a pair of planes with separation l is proportional to l^{-3}, a result as if the force is additive with each pair of atoms exhibiting a van der Waals force, according to the r^{-6} law. This procedure gives the right order of magnitude [9]. As we have shown for the case of H_2^+, although at larger distances, e.g. $R > 16$ au or $R > 8$ Å, the van der Waals force dominates, at distances relevant to STM and AFM experiments, e.g. $R \simeq 3$–6 Å, the van der Waals force is much smaller than the exchange force. However, the polarization does change the amplitude of the electron wavefunction at the separation surface. It results in an increase of the attractive force, similar to Holstein's factor $g = 2\exp(-1/2)$ in the case of the hydrogen molecular ion [19].

3.2. Resonance coupling on metal surfaces

Although the van der Waals force works almost identically for metals and insulators, the exchange force, or resonance force, behaves differently. For metals, the electronic states near the Fermi level are half-filled. At the distances of normal STM operation, these unpaired states are responsible for the exchange force or resonance energy, which makes a net lowering of the total energy of the entire system. In this case, the one-electron picture of the resonance energy is valid, and the tunnelling matrix element provides an appropriate description of the atomic force. On the other hand, for insulators, the exchange coupling results in bonding states as well as antibonding states across the boundary. The net effect of resonance on the total energy is zero. Therefore, only the van der Waals force and the repulsive force are effective.

To make a quantitative treatment, we define a system including a tip and a sample, as shown in figure 6. In the Hartree–Fock formalism, the one-electron Schrödinger equation is identical to equation (2.5), with the potential surface shown in figure 6(*b*). Similar to the treatment of the hydrogen molecular ion, a separation surface is drawn between the tip and the sample, as shown in figure 6(*a*). The exact position of the surface

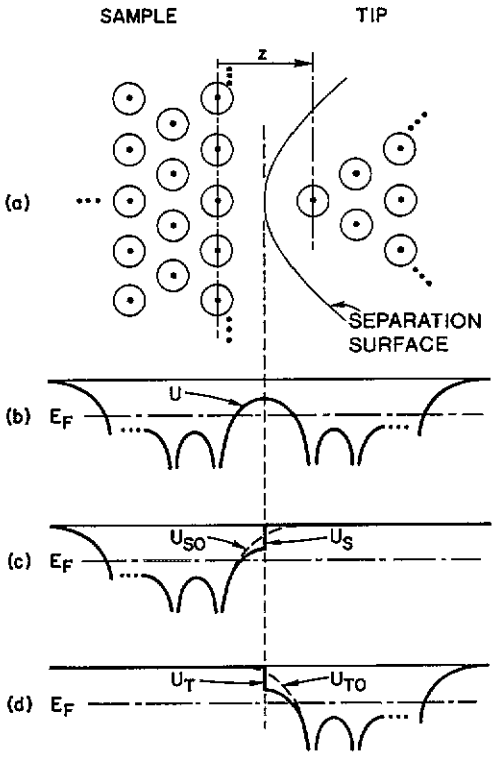

Figure 6. Schematics of the perturbation theory of atomic force between a sample and a tip. (*a*) The geometry of the system. A separation surface is drawn between the tip and the sample. (*b*) The potential of the coupled system. (*c*) The potential surface of the unperturbed Hamiltonian of the sample, U_S, which may be different from the potential surface of the free sample, U_{SO}. (*d*) The potential surface of the unperturbed Hamiltonian of the tip, U_T, which may be different from the potential surface of the free tip, U_{TO}. The effect of the difference between the 'free' tip (sample) potential and the 'distorted' tip (sample) potential can be evaluated using the perturbation method; see [19] and [22].

corresponding Schrödinger equations define the stationary states of the sample and the tip, ψ and χ:

$$(-\tfrac{1}{2}\nabla^2 + U_S)\psi = E\psi \tag{3.1}$$

$$(-\tfrac{1}{2}\nabla^2 + U_T)\chi = E\chi. \tag{3.2}$$

Considering first a single state in the tip and a single state in the sample with the same energy eigenvalue E_0. In the absence of a magnetic field, the Hamiltonian exhibits time-reversal symmetry. Real wavefunctions can be chosen. The derivation of the tunnelling matrix element and the resonance energy is almost identical to the case of H_2^+. If both electrodes are metals, near the Fermi level, every state in the sample side should have a state in the tip side which has the same energy eigenvalue. Therefore, *resonance always exists* even if the two sides are not identical. (In the case of simple molecules, the concept of single-electron resonance does not work if the atoms are not similar [14].) The resonance results in a pair of combined states, $2^{-1/2}(\psi + \chi)$ and $2^{-1/2}(\psi - \chi)$, as well as a splitting of the energy level to $E + M$ and $E - M$, where M is Bardeen's integral in terms of distorted wavefunctions [12]:

$$M = \tfrac{1}{2}\int (\chi\nabla\psi - \psi\nabla\chi)\cdot \mathrm{d}S. \tag{3.3}$$

For the case of the hydrogen molecular ion, the net effect of resonance is a lowering of the total energy. In the case of two pieces of solids, the net effect on the total energy of the coupled system depends on the position of the energy level of unperturbed states. If the energy level of a pair of unperturbed states is much lower than the Fermi level, then both the bonding state and the antibonding state resulting from the exchange interaction are occupied. Therefore, the net energy change of the entire system due to

the exchange interaction between this pair of unperturbed states is zero. For insulators, this is always the case. As a result, for insulators, the van der Waals force and the repulsive force are the major contributors to the observed atomic force. On the other hand, the electronic states on conductor surfaces consist of unpaired electrons. After resonance splitting, only the lower resonance states are occupied. Therefore, a net lowering of the total energy, i.e. a net attractive force due to the exchange coupling, occurs.

3.3. A measurable consequence

In the following, we will derive a relation between the measured tunnelling conductance and the measured atomic force. The major uncertainty is the exact geometry and chemical nature of the end of the tip. Experimentally, the uncertainty is often observed. As we show below, the geometrical arrangement of the atoms near the apex of the tip has a large influence on the magnitude of the force. Therefore, the relation we establish is of order-of-magnitude and functional-dependence nature.

To account for the attractive force in the normal range of STM operation, we consider surface states on the tip near the Fermi level. The states above the Fermi level are normally unoccupied, and therefore do not contribute to the force. For states much lower than the Fermi level, the decay length is much shorter, and the overlap is much weaker. For a single state, the attractive force is

$$F = -\partial M/\partial z. \tag{3.4}$$

For metals, the variation of the tunnelling matrix element M and the density of states ρ over the valence band is small in comparison with their absolute values. A simple relation between the force and the tunnelling current can be established. Assuming that the width of the valence band ε is the same for the tip and the sample, the density of states is $\rho = \varepsilon^{-1}$ for both. The tunnelling conductance is then [22]

$$G = (2\pi)^2 R_K^{-1} \varepsilon^{-2} |M|^2 \tag{3.5}$$

where $R_K = h/e^2 = 25812\ \Omega$ is van Klitzing's constant [23]. Experiments and theoretical studies [24] have shown that, over the entire range of STM operation, the tunnelling conductance varies exponentially with tip–sample distance, $G \propto \exp(-2\kappa z)$, where $\kappa = (2m_e\varphi)^{1/2}/\hbar$ is the decay constant of the surface wavefunction, and φ is the workfunction of the material. Combining equations (3.4) and (3.5), we obtain

$$F = -(2\pi)^{-1} \kappa\varepsilon (G R_K)^{1/2}. \tag{3.6}$$

To establish a quantitative relation between F and G for the entire tip and the entire sample, we have to consider all the states in the tip and the sample. A rigorous treatment is complicated. The following treatment is based on the approximate additivity of atomic force and tunnelling conductance with respect to the atoms of the tip. In other words, the force between the entire tip and the sample can be approximated as the sum of the force between the individual atoms in the tip and the entire sample; so can tunnelling conductivity. Because the tip is made of transition metals, for example, W, Pt and Ir, the tight-bonding approximation, and consequently additivity, is a reasonable assumption. Under this approximation, the total force is

$$F = -(2\pi)^{-1} \kappa\varepsilon \sum_n (G_n R_K)^{1/2} \tag{3.7}$$

where the sum is over all the atoms in the tip. If the atomic resolution of the force is not of concern, the sum can be approximated as an integral over the volume of the tip.

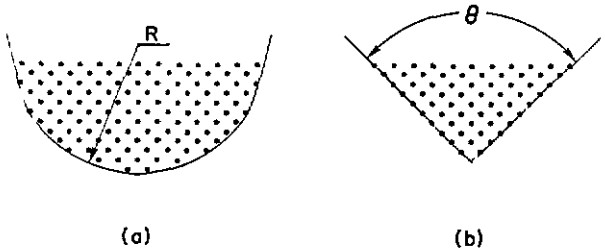

Figure 7. The effect of tip geometry: (*a*) the end of a typical etched metal tip; (*b*) the end of a typical cleaved or cut-out tip.

Denote the distance from the plane of the topmost nuclei of the sample to the apex nucleus of the tip as z_0. For an etched tip, the shape of the end can be represented as a paraboloid (figure 7(*a*)). The cross section at z is $S(z) = 2\pi R(z - z_0)$, where R is the minimum radius of curvature. Denote the tunnelling conductance per unit volume of the tip to the sample as $G_0 \exp(-2\kappa z)$; the total tunnelling conductance is then

$$G = G_0 \int_{z_0}^{\infty} \exp(-2\kappa z) S(z)\, dz = G_0(\pi R/2\kappa^2) \exp(-2\kappa z_0) \tag{3.8}$$

whereas the total force is

$$F = -(2\pi)^{-1}\kappa\varepsilon(G_0 R_K)^{1/2} \int_{z_0}^{\infty} \exp(-\kappa z) S(z)\, dz$$
$$= -(2\pi)^{-1}\kappa\varepsilon(G_0 R_K)^{1/2}(2\pi R/\kappa^2) \exp(-\kappa z_0) = -(2/\pi)\kappa\varepsilon(G R_K)^{1/2}. \tag{3.9}$$

For tips cut mechanically (e.g. with a surgical blade) or cleaved from a brittle material, which exhibit a conical end (figure 7(*b*)), $S(z) \propto (z - z_0)^2$. Similar calculation gives

$$F = -(4/\pi)\kappa\varepsilon(G R_K)^{1/2}. \tag{3.10}$$

By defining a *shape factor* f, which is $f = 2/\pi \simeq 0.637$ for tips with a paraboloidal end and $f = 4/\pi \simeq 1.27$ for tips with a conical end, equations (3.7) and (3.8) can be combined to

$$F = -f\kappa\varepsilon(G R_K)^{1/2}. \tag{3.11}$$

The actual shape of the tip end might be in between. Thus, in general, the shape factor should be a dimensionless number of the order of 1. A comparison with the experiments, using the calculated width of valence bands [25], is shown in figure 8. Line (*a*) in figure 8 represents equation (3.6), with $\kappa = 1.0$ Å^{-1}, and $\varepsilon \simeq 8$ eV. Line (*b*) represents equation (3.11), with $f \simeq 0.64$. Line (*c*) represents equation (3.11), with $f \simeq 1.2$. The data points are from [3]. As shown, the square-root relation as well as the order of magnitude of the absolute values from the theory fit well with experimental data.

3.4. Repulsive force

When the tip is brought even closer to the sample, the repulsive force appears as a result of core–core interaction. A decline of the attractive force is found, as shown by the data

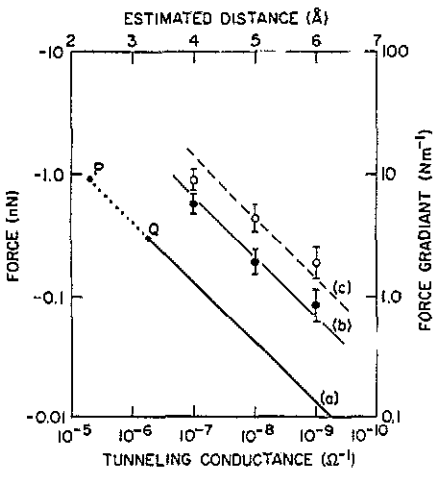

Figure 8. (*a*) The general relation between the atomic force and tunnelling conductance, which is accurate in the attractive-force regime at larger sample–tip distances, e.g. $z > 3$ Å. Parameters used: $\kappa = 1.0$ Å^{-1}, $\varepsilon \simeq 8$ eV. Two points of interest, P and Q, are marked schematically. Below the point Q, the repulsive force dominates, and the linear relation between the atomic force and the square root of tunnelling conductance is no longer correct. Point P is the point of mechanical contact, typically $z < 2.5$ Å. (*b*) Equation (3.11), with $f = 0.64$. (*c*) Equation (3.11), with $f = 1.2$. Experimental data points are taken from two data sets in [1]. The difference in absolute value can be attributed to different tip geometry. As seen, the square-root relation as well as the order of magnitudes of the absolute values from the theory fit well with experimental data.

points in figure 8. In the following, we argue that, as a natural extension of the exponential law of attractive force, the Morse curve is a natural choice based on the following heuristic argument. The energy levels of the core electrons are much deeper (e.g. 10 to 20 eV from the Fermi level), and they have no effect on tunnelling conductance. However, a repulsive force is generated, which also exhibits an exponential dependence on distance, with a decay constant related to the energy level of the core, with a decay constant of roughly 2κ. The sum of the two terms is the well known Morse curve [11]

$$F = -2\kappa U_e\{\exp[-\kappa(z-z_e)] - \exp[-2\kappa(z-z_e)]\} \tag{3.12}$$

where U_e is the binding energy and z_e is the equilibrium distance. One of the advantages of using the Morse curve to represent interatomic forces is that, for periodic surfaces, the sum of the Morse force has a simple analytic form [6]. By assuming a Morse force and a deformable tip, we have reproduced the measured data of the apparent barrier height with reasonable accuracy [5].

4. Conclusions

Based on time-dependent perturbation theory, a fundamental equality between Bardeen's tunnelling matrix element and Heisenberg's resonance energy is established. Applying it to the hydrogen molecular ion, an exceedingly accurate approximate expression for the potential curve in the attractive-force regime is derived. Applying this fundamental relation to STM and AFM, for metals, in the attractive-force regime, an explicit equation between the attractive force and the tunnelling conductance is derived. The equation is found to be in quantitative agreement with experimental results.

Acknowledgments

The author wishes to thank J E Demuth, A Baratoff, J Slonczewski, V Moruzzi and C Herring for helpful discussions. The author is especially grateful to Westinghouse

Science and Technology Center for sending a copy of the 1955 research report [19] of Theodore Holstein, who died in 1985.

Appendix. Transition matrix elements

In this appendix, we present a derivation of the transition matrix element, equation (2.5), which appears in equations (2.13) and (2.14).

A schematic is shown in figure 3. Assume that, at $t < 0$, U_R is turned off. The Schrödinger equation gives the stationary states for the potential U_L. Because we are only interested in the evolution of one state, to simplify the notation, we assume that this state is the ground state, ψ_L:

$$(T + U_L)\psi_L = E_0\psi_L \tag{A1}$$

where $T = -\frac{1}{2}\nabla^2$ is the kinetic energy. At $t > 0$, the right-hand-side potential is turned on. The state ψ_L starts to evolve according to the Schrödinger equation

$$\mathrm{i}\,\partial\Psi/\partial t = (T + U_L + U_R)\Psi. \tag{A2}$$

Expanding Ψ in terms of the eigenfunctions χ_n of the right-hand-side potential, defined by the following stationary-state Schrödinger equation,

$$(T + U_R)\chi_n = E_n\chi_n \tag{A3}$$

the general solution of equation (A2) can be written as:

$$\Psi = \sum_n a_n(t)\chi_n \exp(-\mathrm{i}E_n) \tag{A4}$$

where the functions $a_n(t)$ are to be determined.

Since both equations (A1) and (A3) are real, so simplify the discussion, we require that all the wavefunctions are real. To describe the time evolution of a state that is ψ_L at $t = 0$, we make the *ansatz*

$$a_n(t) = (\chi_n, \psi_L)\exp[-\mathrm{i}(E_0 - E_n)t] + c_n(t) \tag{A5}$$

with $c_n(0) = 0$. Then

$$\Psi = \psi_0 \exp(-\mathrm{i}E_0 t) + \sum_n c_n(t)\chi_n \exp(-\mathrm{i}E_n t). \tag{A6}$$

Substitute equation (A6) into (A2); we obtain exact equations for $c_n(t)$:

$$\mathrm{i}\dot{c}_n(t) = (\chi_n, U_R\psi_L)\exp[-\mathrm{i}(E_0 - E_n)t] + \sum_{k\neq n} c_k(t)(\chi_n, U_L\chi_k)\exp[-\mathrm{i}(E_k - E_n)t]. \tag{A7}$$

For small t, the second term is small. Consider now the first term, i.e. first-order time-dependent perturbation. Except for the term $n = 0$, the exponential factor makes such a swift oscillation that it can be neglected. Denoting the wavefunction χ_0 as ψ_R, equation (A7) becomes

$$\mathrm{i}\dot{c}_n(t) \equiv M = \int_R \psi_L U_R \psi_R \,\mathrm{d}V. \tag{A8}$$

Since U_R is non-vanishing only in the right half of the space, the integral in equation

(A8), i.e. the transmission matrix element M, is evaluated only in the right half of the space.

In the following, we convert the volume integral to a surface integral using the Schrödinger equations (A1) and (A3). Using equation (A3), and noticing that E_0 is a constant,

$$M = \int_R \psi_L(E_0 - T)\psi_R \, dV = \int_R (\psi_R E_0 \psi_L - \psi_L T \psi_R) \, dV. \tag{A9}$$

By using equation (A1), and noticing that in the right half of the space, $U_L = 0$, we obtain

$$M = \int_R (\psi_R T \psi_L - \psi_L T \psi_R) \, dV = -\frac{\hbar}{2} \int_R (\psi_R \nabla^2 \psi_L - \psi_L \nabla^2 \psi_R) \, dV. \tag{A10}$$

Finally, using the Green theorem, the volume integral in equation (A10) is converted into a surface integral, i.e. the Bardeen integral [12]:

$$M = \frac{\hbar}{2} \int (\psi_R \nabla \psi_L - \psi_L \nabla \psi_R) \cdot dS \tag{A11}$$

where the integral is carried out on the separation surface, which is the mid-plane in the hydrogen molecular ion problem.

An observation into the behaviour of the wavefunctions reveals immediately that the value of this matrix element is negative. In fact, ψ_L varies with z as $\exp(-z)$; the z derivative of it is negative. The derivative in the second term is positive, and the negative sign makes its value equal to that of the first term.

By starting with a right-hand-side wavefunction, we reach the same transition matrix element (without changing the sign), because when the Green theorem is applied to the left-hand side, the direction of the norm is reversed.

References

[1] Binnig G, Rohrer H, Gerber C and Weibel E 1982 *Phys. Rev. Lett.* **49** 57
Binnig G and Rohrer H 1987 *Rev. Mod. Phys.* **56** 615

[2] Binnig G, Quate C F and Weibel C 1986 *Phys. Rev. Lett.* **56** 930

[3] Dürig U, Gimzewski J K and Pohl D W 1986 *Phys. Rev. Lett.* **57** 2403
Dürig U, Züger O and Pohl D W 1988 *J. Microsc.* **152** 259

[4] Solar J M, Baro A M, Garcia N and Rohrer H 1986 *Phys. Rev. Lett.* **57** 444
Mamin H J, Ganz E, Abraham D W, Thomson R E and Clarke J 1986 *Phys. Rev.* B **34** 9015
Pethica J B and Sutton A P 1988 *J. Vac. Sci. Technol.* A **8** 2490
Pethica J B and Oliver W C 1987 *Phys. Scr.* **19** 61

[5] Chen C J and Hamers R J 1991 *J. Vac. Sci. Technol.* B **9**

[6] Chen C J 1990 *Phys. Rev. Lett.* **65** 448; 1990 *Phys. Rev.* B **42** 8841; 1991 *J. Vac. Sci. Technol.* A **9** 44; 1990 *Mater. Res. Soc. Symp. Proc.* **159** 289

[7] Tersoff J and Hamann D 1985 *Phys. Rev.* B **31** 805
Tersoff J 1989 *Phys. Rev.* B **39** 1052
Lang N D 1985 *Phys. Rev. Lett.* **55** 230; 1986 *Phys. Rev. Lett.* **56** 1164

[8] Landau L D and Lifshitz E M 1977 *Quantum Mechanics* 3rd edn (Oxford: Pergamon) pp 339–41
Pauling L and Wilson E B 1935 *Introduction to Quantum Mechanics* (New York: McGraw-Hill) pp 384–6
Lifshitz E M and Pitaevskii L P 1980 *Statistical Physics II, Theory of the Condensed State* (Oxford: Pergamon) pp 331–47

[9] Girard C, Van Labeke D and Vigoureux J M 1989 *Phys. Rev.* **40** 12133
Gould S A C, Burke K and Hansma P K 1989 *Phys. Rev.* **40** 5363
Moiseev Yu N, Mostepanenko V M, Panov V I and Sokolov I Yu 1988 *Phys. Lett.* **132A** 354
[10] Rose J H, Ferrante J and Smith J R 1981 *Phys. Rev. Lett.* **47** 675
Rose J H, Smith J R and Ferrante J 1983 *Phys. Rev.* B **28** 1835
[11] Slater J C 1963 *Quantum Theory of Molecules and Solids* vol 1 (New York: McGraw-Hill) pp 1–40
[12] Bardeen J 1961 *Phys. Rev. Lett.* **6** 57
[13] Heisenberg W 1926 *Z. Phys.* **38** 411. For a pedagogical explanation, see either Pauling L and Wilson E B 1935 *Introduction to Quantum Mechanics* (New York: McGraw-Hill) pp 314–25 or Feynman R P 1965 *The Feynman Lectures on Physics, Quantum Mechanics* (Reading, MA: Addison-Wesley) pp 10-1 to 10-6
[14] Pauling L 1977 *The Nature of the Chemical Bond* 3rd edn (Ithaca, NY: Cornell University Press)
[15] Rosen N 1931 *Phys. Rev.* **38** 2099
Dickinson B N 1933 *J. Chem. Phys.* **1** 317
[16] Tekman E and Ciraci S 1988 *Phys. Scr.* **38** 486
Ciraci S, Baratoff A and Batra I P 1990 *Phys. Rev.* B **41** 2763
[17] Pauling L and Wilson E B 1935 *Introduction to Quantum Mechanics* (New York: McGraw-Hill) pp 195–8
[18] Oppenheimer J R 1928 *Phys. Rev.* **13** 66
[19] Holstein T 1955 *Westinghouse Research Report* 60-94698-3-R9. Copies of this can be obtained from Westinghouse Science and Technology Center, Pittsburgh, Pennsylvania, USA. A brief description of the results therein can be found in Herring C 1962 *Rev. Mod. Phys.* **34** 631
[20] Bates D R, Ledsman K and Stewart A L 1953 *Phil. Trans. R. Soc.* **246** 215
[21] Flores F, Martin-Rodeno A, Goldberg E C and Duran J C 1988 *Nuovo Cimento* D **10** 303
[22] Chen C J 1988 *J. Vac. Sci. Technol.* A **6** 319; 1991 *Mod. Phys. Lett.* B **5** 107
[23] von Klitzing K 1986 *Rev. Mod. Phys.* **58** 519
von Klitzing K, Dorda G and Pepper M 1980 *Phys. Rev. Lett.* **45** 494
[24] Binnig G, Rohrer H, Gerber C and Weibel E 1982 *Appl. Phys. Lett.* **40** 178
Binnig G, Garcia N and Rohrer H 1984 *Phys. Rev.* B **30** 4816
Gimzewski J K and Möller R 1987 *Phys. Rev.* B **36** 1284
Binnig G, Garcia N, Rohrer H, Soler J M and Flores F 1984 *Phys. Rev.* B **30** 4816
Coombs J H, Welland M E and Pethica J B 1988 *Surf. Sci.* **198** L353
[25] Moruzzi V L, Janak J F and Williams A R 1978 *Calculated Electronic Properties of Metals* (New York: Pergamon)